coatings

MDPI

Article

Original Blue Light-Emitting Diphenyl Sulfone Derivatives as Potential TADF Emitters for OLEDs

Margarita Anna Zommere [1], Natalija Tetervenoka [1], Anna Pidluzhna [1], Raitis Grzibovskis [1], Dovydas Blazevicius [2], Gintare Krucaite [2], Daiva Tavgeniene [2], Saulius Grigalevicius [2] and Aivars Vembris [1,3,*]

[1] Institute of Solid State Physics, University of Latvia, LV-1063 Riga, Latvia; margarita.zommere@cfi.lu.lv (M.A.Z.); natalija.tetervenoka@cfi.lu.lv (N.T.); anna.pidluzhna@cfi.lu.lv (A.P.); raitis.grzibovskis@cfi.lu.lv (R.G.)
[2] Department of Polymer Chemistry and Technology, Kaunas University of Technology, 51424 Kaunas, Lithuania; dovydas.blazevicius@ktu.lt (D.B.); gintare.krucaite@ktu.lt (G.K.); daiva.tavgeniene@ktu.lt (D.T.); saulius.grigalevicius@ktu.lt (S.G.)
[3] Faculty of Science and Technology, University of Latvia, LV-1004 Riga, Latvia
* Correspondence: aivars.vembris@cfi.lu.lv

Abstract: Organic light-emitting diodes (OLEDs) have emerged as one of the dominant technologies in displays due to their high emission efficiency and low power consumption. However, the development of blue color emitters has fallen behind that of red and green emitters, posing challenges in achieving optimal efficiency, stability, and accessibility. In this context, thermally activated delayed fluorescence (TADF) emitters hold promise as a potential solution for cost-effective, exceptionally efficient, and stable blue OLEDs due to their potential high efficiency and stability. TADF is a principle where certain organic materials can efficiently convert both singlet and triplet excitons, theoretically achieving up to 100% internal quantum efficiency. This research focused on diphenyl sulfone derivatives with carbazole groups as TADF compounds. Quantum chemical calculations and photoluminescence properties show the potential TADF properties of the molecules. New materials exhibit glass transition temperatures that would classify them as molecular glasses. Depending on the structure of the molecule, the photoluminescence emission is in the blue or green spectral region. Organic light-emitting diodes were fabricated from neat thin films of emitters by the wet casting method. The best performance in the deep blue emission region was achieved by a device with a turn-on voltage of 4 V and a maximum brightness of 178 cd/m^2. In the blue-green emission region, the best performance was observed by an OLED with a turn-on voltage of 3.5 V, reaching a maximum brightness of 660 cd/m^2.

Keywords: diphenyl sulfone derivatives; thermally activated delayed fluorescence; blue emitters; organic light-emitting diodes

check for updates

Citation: Zommere, M.A.; Tetervenoka, N.; Pidluzhna, A.; Grzibovskis, R.; Blazevicius, D.; Krucaite, G.; Tavgeniene, D.; Grigalevicius, S.; Vembris, A. Original Blue Light-Emitting Diphenyl Sulfone Derivatives as Potential TADF Emitters for OLEDs. *Coatings* **2024**, *14*, 1294. https://doi.org/10.3390/coatings14101294

Academic Editor: Igor V. Khudyakov

Received: 8 August 2024
Revised: 6 September 2024
Accepted: 7 October 2024
Published: 11 October 2024

Copyright: © 2024 by the authors. Licensee MDPI, Basel, Switzerland. This article is an open access article distributed under the terms and conditions of the Creative Commons Attribution (CC BY) license (https://creativecommons.org/licenses/by/4.0/).

1. Introduction

Organic light-emitting diodes (OLEDs) are widely used in displays due to their high efficiency, lower production costs, fast response time, and flexibility [1–3]. While red and green pixel efficiency is relatively high, the efficiency of blue light OLEDs is limited by the instability of the emitters due to the high excitation energy and high energetic barriers at the interface, resulting in the higher operating voltages of devices [4–7]. However, this low-efficiency issue in purely fluorescent devices has been effectively resolved by using noble metal-based organometallic phosphors, allowing for the creation of blue OLEDs with external quantum efficiencies (EQEs) exceeding 30% [8,9]. Nonetheless, persistent limitations such as operational lifetime, high cost caused by limited availability, and environmental concerns of noble metal phosphors [10–12] paved the way for thermally activated delayed fluorescence (TADF) materials, which have been proposed as one of

the potential solutions [13–18]. TADF materials represent the latest generation of OLED technology, where 100% of the electrically excited states are converted into light due to the reverse intersystem crossing caused by the thermal upconversion of excitons from the triplet excited state to the singlet excited state. For this process to be successful, it is essential to ensure that there is minimal overlap between the highest occupied molecular orbital (HOMO) and lowest unoccupied molecular orbital (LUMO), resulting in the smallest possible energy difference between the singlet and triplet excited states [19,20].

Currently, there is a significant focus on solution-processable TADF organic LEDs due to their cost-effectiveness, simpler design structure, and ability to be expanded for use in large-scale displays [21–24]. In previous research, it has been shown that diphenyl sulfone derivatives with carbazole groups have demonstrated promising results as TADF emitters [23,25–27]. The benefit of the diphenyl sulfone acceptor part comes from its shape—the sulfonyl group forms a tetrahedron, which stops the molecules from connecting too much. This leads to a strong charge transfer inside the molecule [28]. Carbazole, as an organic material, possesses four key advantages that are noteworthy. These include its cost-effectiveness; its capacity for easy functionalization at the nitrogen atom, allowing for adjustments of various properties without affecting the core structure; its multiple linkage positions along the carbazole backbone; and its aromatic characteristics that grant stability across a wide range of conditions. It is expected that [3,3′]bicarbazole, [2,3′]bicarbazole, and carbazole derivatives with arylamino substitutions could potentially exhibit enhanced properties when employed as electron-donating components in TADF emitters. This research was conducted for original molecules with diphenyl sulfone derivatives with carbazole groups and aimed to find potential blue light emitters for OLEDs that would be suitable for the spin-coating method [29–31].

2. Materials and Methods

2.1. Sample Preparation

Anhydrous tetrahydrofuran (THF) was used to prepare solutions for the optical measurements. Solutions with 10^{-5} M concentration were used for UV–Vis absorption measurements, while solutions with 10^{-4} M concentration were used to acquire emission data. As mentioned earlier, TADF compounds are greatly influenced by the presence of oxygen. Therefore, it is crucial to degas the solution by replacing oxygen with argon gas. The degassing process was carried out in an argon glove box.

Thin films for investigating the optical properties of the compounds were fabricated by spin-coating from THF solution at a compound concentration of 20 mg/mL onto a quartz substrate. The rotation speed was adjusted to 800 rpm with an acceleration of 800 rpm per second for a duration of 1 min. After spin-coating, the samples were placed onto a hotplate at 100 °C and kept there for 15 min. The samples for energy level determination were made on ITO-covered glass substrates (Präzisions Glas and Optik GmbH, Iserlohn, Germany, 15 Ω/square). Compounds were dissolved in THF with a concentration of 30 mg/mL and spin-coated to obtain a film with a thickness of around 500 nm. The thickness of the films was measured by the Surface Profile Measuring System Veeco Dektak 150 (Bruker, Karlsruhe, Germany). The spin-coating parameters were as follows: an acceleration of 500 rpm/s, a rotation speed of 500 rpm, and a spinning time of 60 s. Afterwards, the samples were dried on a hotplate at 130 °C for 15 min to eliminate the remaining solvent. The intrinsic photoconductivity measurements were performed on the same samples as those for energy level determination, but on top of the organic layer, semitransparent aluminum with a thickness of 30 nm was deposited.

For the fabrication of OLED systems, the concentration of the emitter layer was chosen to achieve a layer thickness of approximately 50 nm. The concentration of the solutions varied between 5 and 7 mg/mL, which was applied to the substrate at a speed of 2000 rpm with an acceleration of 2000 rpm/s. Subsequently, the samples were heated at 100 °C for 15 min.

2.2. Investigation Methods

Thermogravimetric analysis (TGA) was performed on a TGAQ50 apparatus (TA Instruments, Alzenau, Germany). The TGA and DSC curves were recorded in a nitrogen atmosphere at a heating rate of 10 °C/min. Differential scanning calorimetry (DSC) measurements were carried out using a Bruker Reflex II thermos system, Ettlingen, Germany.

Optical measurements were conducted on both solutions and thin films. The samples were prepared within a controlled environment using both a degassed and non-degassed THF solvent in a glove box under an argon atmosphere. Additionally, OLEDs were constructed to evaluate the performance of these compounds.

Thin films for optical measurements were prepared using the spin-coating method with a Laurell spin-coater. Absorption measurements were conducted using a Cary 7000 spectrometer, Agilent, Santa Clara, CA, USA. Emission spectra, photoluminescence quantum yields, and kinetics were determined using a photoluminescence spectrometer FLS1000 (Edinburgh Unstruments Ktd, Edinburgh, UK). Fluorescence spectra were measured for solutions and thin films at room temperature. Phosphorescence was measured for thin films at 77 K with a time delay of 100 µs. The brightness and CIE 1931 coordinates of the OLEDs were measured in a glove box using a Konica Minolta Chroma Meter, Osaka, Japan. The current–voltage characteristics of the OLEDs were measured with a Keithley 2450 multimeter, Cleveland, OH, USA, and the voltage source used was a Keithley 2450 unit. The electroluminescence (EL) spectrum was recorded with a calibrated Ocean Optics STS UV/VIS spectrometer, Orlando, FL, USA. The CIE 1931 coordinates and spectrum provided in this study were acquired under the conditions of the maximum achieved brightness.

The photoemission spectroscopy (PES) method within a vacuum environment of approximately 1×10^{-5} mBar was employed to determine the ionization energy levels. The experimental setup consisted of the ENERGETIQ Laser-Driven Light Source (LDLS EQ-99) (Wilmington, MA, USA) white light source, the Spectral Products DK240 1/4 m monochromator (Putnam, CT, USA), and the Keithley 617 electrometer. The UV radiation was focused on a 5×5 mm^2 area on the sample surface. The distance between the electron-collecting copper electrode and the sample was maintained around 2 cm. Additionally, we applied a voltage of 50 V between the sample and electrode to amplify the obtained signal amplitude. Our measurement range spanned from 3.5 to 6.5 eV, with a precise step size of 0.05 eV. In PES measurements, the photoemission yield $Y(h\nu)$ can be calculated as

$$Y(h\nu) = \frac{J(h\nu)}{P(h\nu)} \quad (1)$$

where $J(h\nu)$ is the measured current (the number of emitted electrons), and $P(h\nu)$ is the number of incident photons with the energy of $h\nu$ [32]. The relation between photoemission yield and ionization energy E_{ioniz} or work function can be expressed as a power law

$$Y(h\nu) = a(h\nu - E_{ioniz})^n \quad (2)$$

where a is a constant showing the amplitude of the signal, and $n = 1...3$ depending on the studied materials [33]. In the case of semiconductors, $n = 2.5...3$ [34,35]. In this work, we used $n = 2.5$ as it gave a better approximation than $n = 3$. To obtain the ionization energy level of the material, $Y^{1/n}(h\nu)$ was calculated, and its dependence on photon energy was plotted. The linear part of the $Y^{1/n}(h\nu)$ curve was extrapolated until $Y^{1/n}(h\nu) = 0$. The obtained value was considered the ionization energy of the material.

The equipment for photoconductivity measurements was the same as that in photoelectron emission spectroscopy. In this case, there was no copper electrode 2 cm from the sample surface. Instead, one electrical contact was connected to ITO, while the other was connected to the Al electrode. The light was focused on a 3×3 mm^2 area where ITO and Al overlapped. For the pure films, photoconductivity was used to determine the energy gap (E_g) between the material ionization energy level and electron affinity level. Knowing

the energy gap and the ionization energy (I) level value, it was possible to calculate the electron affinity level value:

$$EA = I - E_g \quad (3)$$

To evaluate the orbital position in the molecules and the highest occupied molecular orbital (HOMO) and lowest unoccupied molecular orbital (LUMO), overlapping density functional theory (DFT) calculations were performed by using the Gaussian 09 program [36] at the B3LYP functional and 6-31G(d,p) base in the gas phase. The optimized molecular geometries were confirmed to be minimum-energy conformations by computing vibrational frequencies at the same level.

2.3. OLED Fabrication

OLED samples with the following structure were prepared: ITO/PEDOT:PSS (40 nm)/emitter (50 nm)/TPBi (25 nm)/LiF (1 nm)/Al (120 nm). The substrate used was indium tin oxide (ITO) with a resistivity of 50 Ω/square (Präzisions Glas and Optik GmbH). The ITO substrates underwent a cleaning process involving chloroform, acetone, and isopropanol solvent sonication, with each sonication step lasting for 15 min. After the cleaning process, the substrates were dried using a flow of nitrogen (N_2). To ensure substrate cleanliness, a 20 min ozone treatment using the UV/Ozone Pro Cleaner™ (La Jolla, CA, USA) was performed. Following ozonation, a hole injection and ITO smoothing layer, poly (3,4-ethylenedioxythiophene) polystyrene sulfonate (PEDOT:PSS), was spin-coated at 2000 rpm with an acceleration of 2000 rpm/s. The coated layer was then heated for 20 min at 125 °C. The emitter layer was also deposited by using the spin-coating technique with the same rotation speed and acceleration as those for PEDOT:PSS. However, this time, the samples were prepared in a glove box and heated there for 15 min at 100 °C. Subsequently, the samples were transferred to a vacuum chamber in a sealed container for the thermal evaporation of the remaining OLED layers. In the vacuum chamber, 2,2′,2″-(1,3,5-benzinetriyl)-tris(1-phenyl-1-H-benzimidazole) (TPBi), lithium fluoride (LiF), and aluminum (Al) were evaporated at a pressure of 6×10^{-6} Torr.

3. Results and Discussion

3.1. Studied Materials

The synthesis of bicarbazole-based materials was carried out by the three-step synthetic route, as shown in Scheme 1. 3,3-bicarbazole (2) was obtained by oxidizing carbazole using iron (III) chloride. Various 9-alkyl-9′H-3,3′-bicarbazoles (3–6) were obtained by an N-alkylation reaction between bicarbazole and the corresponding alkyl-bromides using potassium hydroxide and potassium carbonate in tetrahydrofuran (THF). These intermediate materials were purified by silica gel chromatography using a mixture of THF and hexane as an eluent with the overall yields being in the range of 40% to 44%. The last step was the nucleophilic aromatic substitution of alkylated bicarbazole with 4,4′-difluorobenzophenone. The mentioned reaction was carried out in DMSO using vacuum-dried potassium carbonate as a base and resulted in objective materials DB16, DB17, DB18, DB22, DB26, and DB27. All objective derivatives were purified by silica gel chromatography using a mixture of tetrahydrofuran (THF) and hexane as an eluent. The structures of the new materials were identified by mass spectrometry and NMR spectroscopy (Supplementary Figures S1–S6). The data were found to be in good agreement with the proposed structure.

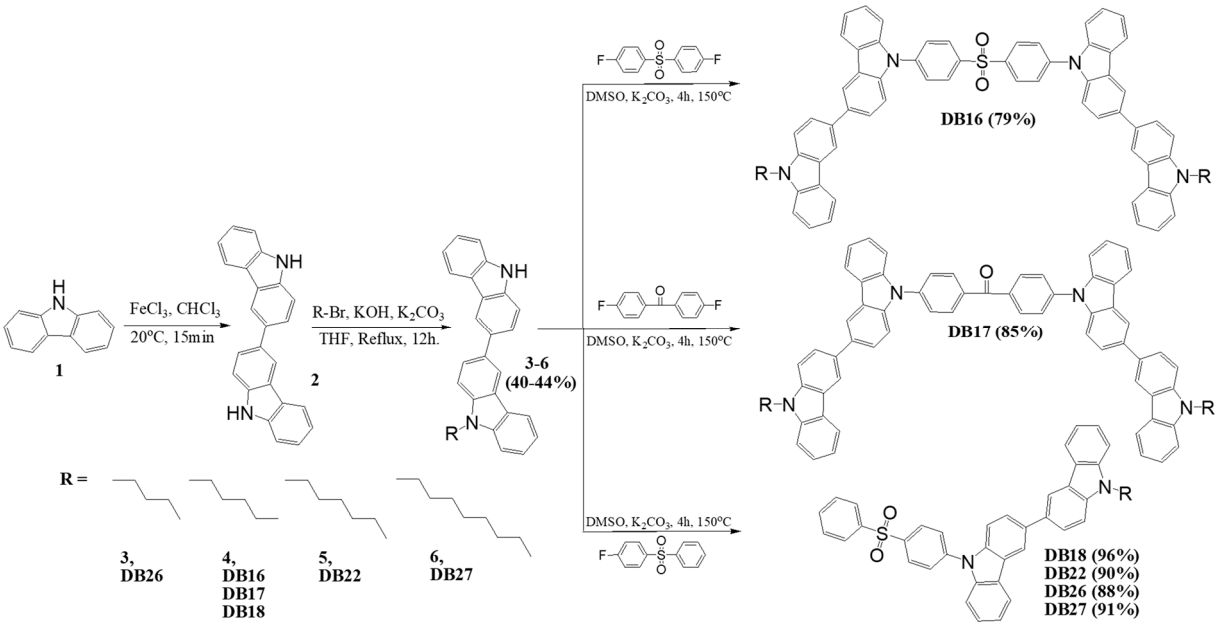

Scheme 1. Synthesis of new emitting materials.

The behavior under the heating of the synthesized materials DB16, DB17, DB18, DB22, DB26, and DB27 was studied using differential scanning calorimetry (DSC) and thermogravimetric analysis (TGA) by heating samples under nitrogen atmosphere. It was established that the objective compounds demonstrated very high thermal stability. The temperature of 5% weight loss (T_d) for derivative DB16 was 462 °C, as shown in Figure S1. Compound DB17 was also stable under heating with a T_d of 423 °C. Materials DB18, DB22, DB26, and DB27, which were substituted with only one 9-alkylated bicarbazole fragment, demonstrated similarly good thermal stability, with T_d reaching 380 °C, 396 °C, 421 °C, and 391 °C, respectively, as confirmed by TGA with a heating rate of 10 °C/min (see Supplementary Figures S7–S12).

The DSC thermo-grams of the second heating of the compounds DB16, DB17, DB18, DB22, DB26, and DB27 are presented in Figure 1. It can be clearly seen from the curves that the new derivatives have glass transition temperatures that directly correlate with the length of the alkyl substituent. For example, the butyl group having material DB26 demonstrated a very high glass transition temperature of 111 °C. Pentyl-, hexyl-, and octyl-substituted compounds DB18, DB22, and DB27 showed slightly lower glass transition temperatures of 100 °C, 89 °C, and 77 °C, respectively. Materials DB16 and DB17, each containing two bicarbazole fragments, exhibited highly morphologically stable amorphous layers with glass transition temperatures of 147 °C and 133 °C, respectively. Both the TGA and DSC results are compiled in Table 1. Overall, these findings confirm that the materials are well suited for application in amorphous electroactive layers of OLED devices.

Table 1. Thermal properties of newly synthesized materials.

Compound	T_d, °C	T_g, °C
DB16	462	147
DB17	423	133
DB18	380	100
DB22	396	89
DB26	421	111
DB27	391	77

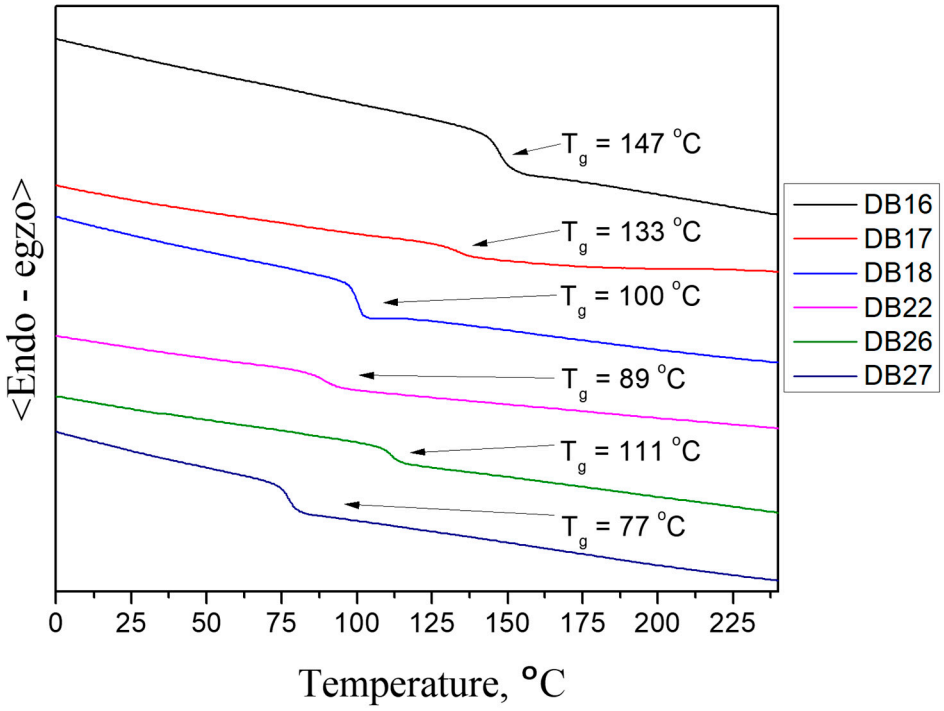

Figure 1. Second heating curves of DSC of compounds DB16, DB17, DB18, DB22, DB26, and DB27. Heating rate: 10 °C/min.

3.2. Theoretical Calculations

The molecular orbital positions of objective molecules DB16, DB17, and DB22 are shown in Figure 2. Visualizations of orbitals of other materials can be seen in Figure S13. For all molecules, the HOMO is located on the carbazole fragment, while the LUMO is located on the diphenyl sulfone or benzophenone moieties. A small molecular orbital overlap was observed, indicating the possibility of a TADF process in these materials.

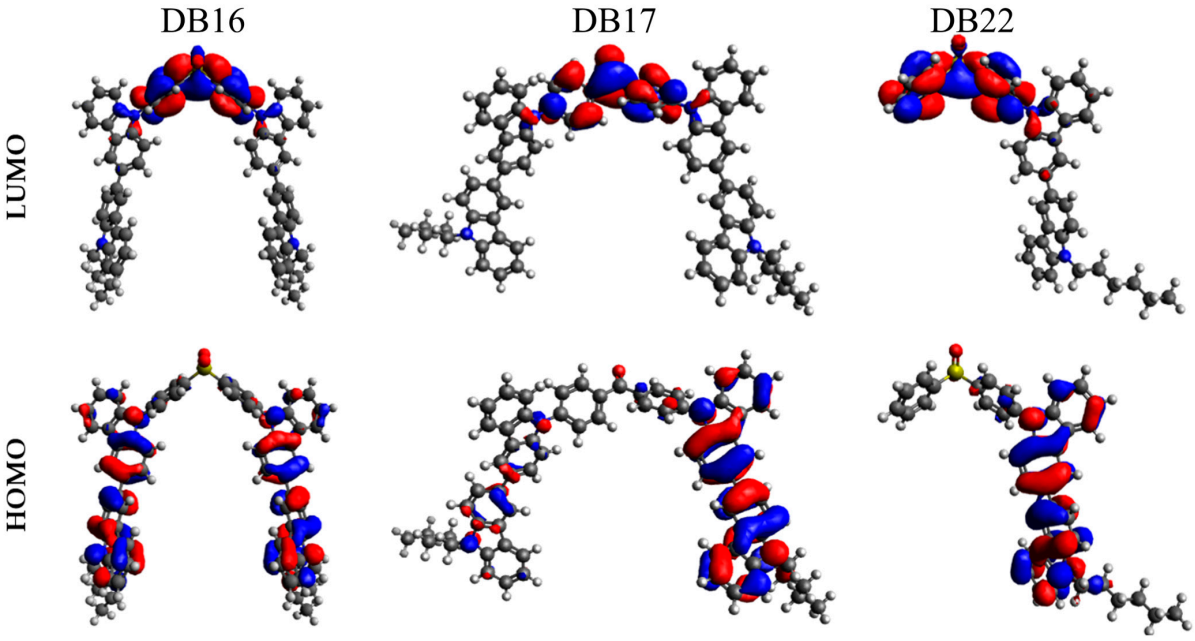

Figure 2. Molecular orbital positions of HOMO and LUMO levels for molecules DB16, DB17, and DB22.

3.3. Photophysical Properties

Absorption spectra in solution exhibit several absorption bands (see Figure 3a and Table S1). High-energy bands below 300 nm are related to the π–π* and n–π* transition. For DB16 and DB17, the extinction coefficient is the largest compared to that of other molecules. Those molecules also have twice as many carbazole groups which means that high-energy bands are mostly attributed to the local excited states of carbazole. Intramolecular charge transfer (CT) is the origin of the low-energy absorption band around 340 to 360 nm. Molecules with nonsymmetrical carbazole groups have similar second absorption bands with a maximum of around 345 nm, and the length of alkyl chains has only a small influence (within a few nanometers) on the absorption spectra. This can be expected because alkyl chains should not change the optical properties but only the morphology of thin films. The DB16 molecule with symmetrical carbazole groups has a small red shift (around 5 nm) which is a result of the presence of symmetry. But for the DB17 molecule, the second absorption band is even more red-shifted and much broader with several peaks above it. The red shift observed in DB17 can be attributed to the alteration in acceptor group properties resulting from the substitution of a sulfur atom with carbon. The benzophenone fragment has strong electron acceptor properties. Consequently, a stronger electron acceptor group will cause a shift in electron transition energy towards lower values, leading to a red shift in absorption spectra.

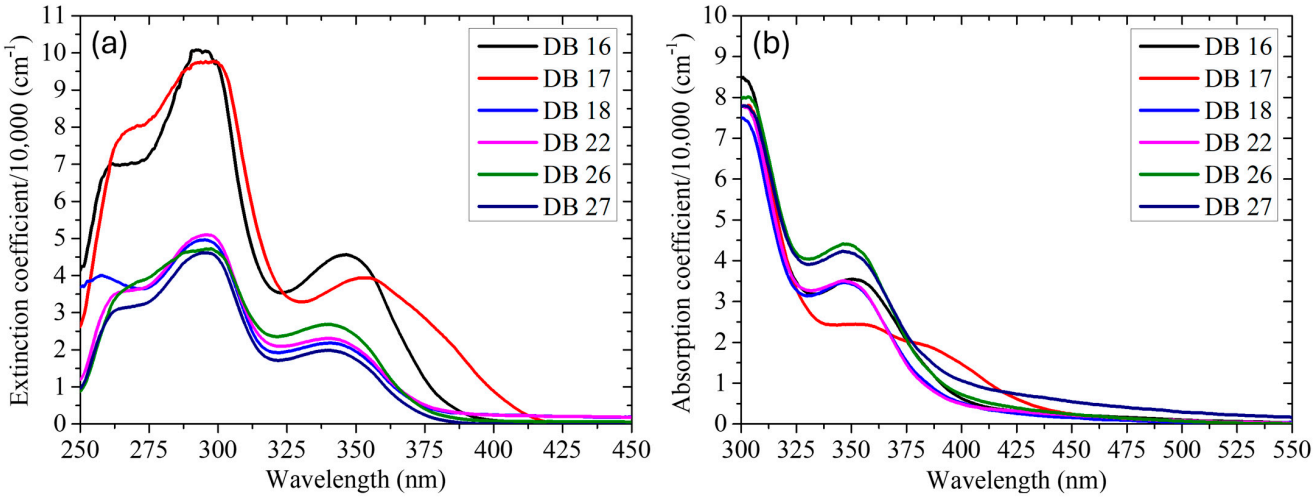

Figure 3. Absorption and emission spectra of studied compounds in THF solution (**a**) and thin films (**b**).

The absorption spectra in pure thin films have the same shape of absorption bands with the 5 nm red shift in the lower energy band (see Figure 3b and Table S1). So, small changes can be explained by alkyl chains which should prevent strong interactions of the molecules, thus reducing quenching.

The solutions were excited using the wavelength of the absorption peak, resulting in the maximum emission intensity. All compounds, except for DB17, exhibit luminescence in the blue spectral region (see Figure 4 and Table S1). DB27 has the longest alkyl sidechains, which explains the matching solution and thin film spectra. Adding alkyl chains protects the active CT (charge transfer) part between the molecule acceptor and donor when molecules are closely packed in the amorphous phase. The emission is the most red-shifted for the compound with benzophenone (DB17) as the electron acceptor group.

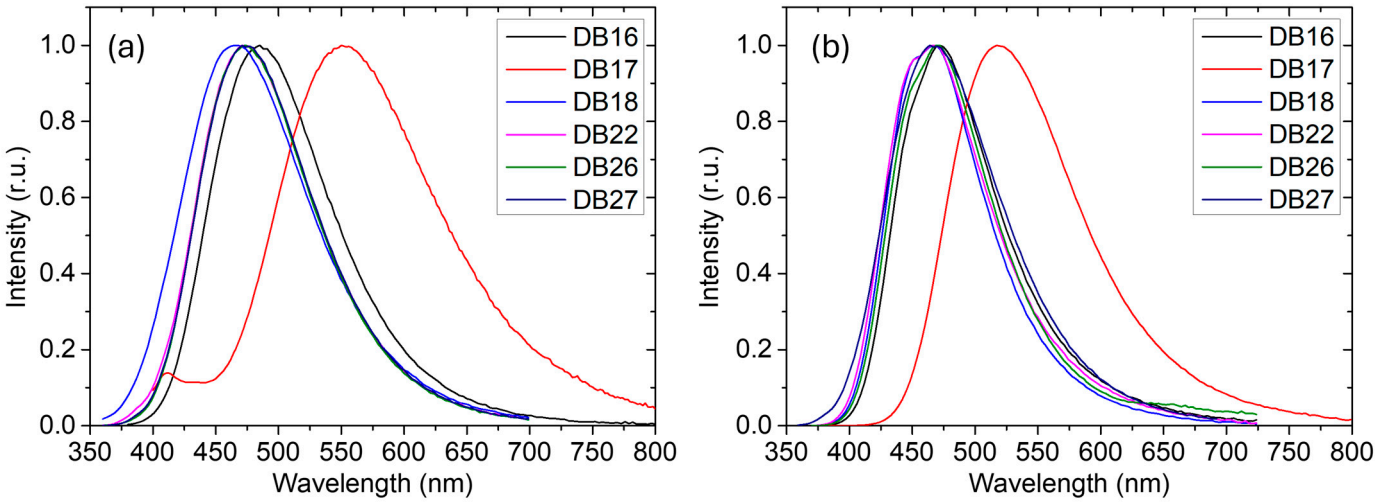

Figure 4. Emission spectra of (**a**) degassed solutions and (**b**) thin films.

The low-intensity blue emission peak, with a maximum around 410 nm, may originate from the benzophenone component of the molecule [37]. However, the high level of intermolecular interaction prevents the observation of this emission from the benzophenone component in the pure thin film.

In TADF, population transfer from the triplet state is essential, and any process that reduces the population in the triplet state will result in a reduced intensity of TADF emission. The presence of oxygen for such compounds is critical because it interacts with the triplet states and significantly reduces the emission intensity. Molecular oxygen has a low triplet ground state and will, therefore, remove the population from the first excited triplet state through energy transfer, thus extinguishing the TADF emission [38]. Therefore, to demonstrate the TADF properties of the investigated compounds, their optical properties were examined in both degassed and non-degassed solvents [39]. The emission spectra (see Figure 5) clearly demonstrate that the solutions prepared from degassed THF exhibit stronger photoluminescence. This consistent trend was observed across all tested samples (see Supplementary Figure S14), providing compelling evidence for the TADF properties of these compounds. Importantly, the recorded spectra remain unchanged, indicating that the emission mechanism primarily involves singlet states.

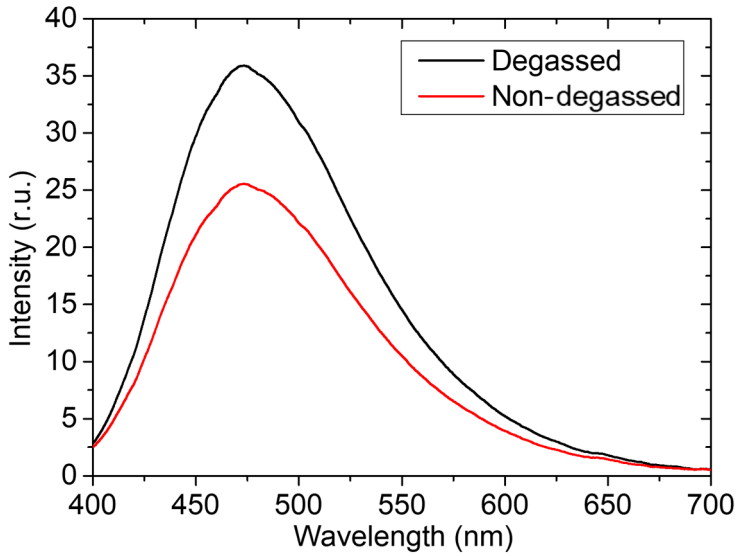

Figure 5. Emission spectra of degassed and non-degassed solutions of DB18 compound.

Photoluminescence quantum yields were measured for both degassed and non-degassed solvent solutions, as well as for thin films prepared from degassed solvent (Table 2). As shown in Table 2, five out of six materials demonstrated higher PLQY values in the degassed solvent (ranging from 17.1% to 53.3%) compared to the non-degassed solvent (ranging from 8.5% to 32.8%), clearly indicating the TADF nature of the investigated compounds. However, material DB27, which has the longest aliphatic substituent, was an exception. The extended aliphatic chain may have created a protective microenvironment around the chromophores, thereby reducing the quenching effect even in the presence of oxygen. Additionally, the benzophenone-based material DB17 exhibited a significantly lower PLQY compared to the diphenyl sulfone-based derivatives. This difference can be attributed to the stronger electron-withdrawing nature of benzophenone, its higher propensity for intersystem crossing, and increased conformational flexibility. These factors collectively promote nonradiative decay processes in benzophenone-based materials, leading to a reduced PLQY compared to diphenyl sulfone-based materials. Additionally, it was observed that the compounds exhibit relatively high potential, given the notable efficiency achieved. A comparison between the PLQY of the solution and the thin film reveals a significantly lower PLQY in the pure thin films. This can be attributed to the close proximity of the molecules in the thin film, resulting in the quenching of the excited states due to interactions and a subsequent decrease in luminescence intensity.

Table 2. PLQY in thin films and solutions. Singlet and triplet energies [a]. Estimated from onset of fluorescence. [b]. Estimated from onset of phosphorescence.

Compound	Pure Thin Films			THF Solution	PLQY		
					Thin Films 20 mg/mL	THF Solution 10^{-4} M	
	E_S [a] (eV)	E_T [b] (eV)	ΔE_{ST} (eV)	τ_p (ns)	Degassed THF (% ± 1%)	Non-Degassed (% ± 1%)	Degassed (% ± 1%)
DB16	3.03	2.81	0.22	15.21	15.6	37.0	52.8
DB17	2.76	2.62	0.14	5.88	12.5	9.3	17.1
DB18	3.05	2.88	0.17	13.42	16.5	24.7	40.6
DB22	3.08	2.90	0.18	10.38	8.5	36.1	37.9
DB26	3.05	2.87	0.18	13.43	32.8	38.2	53.3
DB27	3.07	2.89	0.18	13.53	56.5	24.0	53.4

The emission spectra of thin films at room temperature and 77 K are presented in Supplementary Figure S15. The singlet energy (E_S) was calculated from the fluorescence onset of each compound and estimated to be between 2.76 and 3.08 eV. Similarly, the respective triplet energies (E_T) of the compounds, calculated from the phosphorescence onset, were estimated to be between 2.62 and 2.90 eV (refer to Table 2). The length of the alkyl chain did not significantly influence the singlet and triplet energy values, as observed in the emission spectra of the compounds. Notably, DB17 exhibited the smallest triplet and singlet energies, along with a red-shifted emission spectrum. The difference in the singlet–triplet energy bandgap (ΔE_{ST}) values for the compounds ranged from 0.14 to 0.22 eV, indicating a potential reverse intersystem crossing (RISC) phenomenon [40]. The photoluminescence kinetics of the compounds in the degassed THF solvent displayed two decay exponents, while in the non-degassed solvent, one decay with an almost untraceable second decay was primarily observed (see Supplementary Figure S16). The presence of oxygen reduced the number of triplet excited states capable of undergoing reverse intersystem crossing. The prompt component of the photoluminescence lifetimes ranged from 5.88 to 15.21 ns (see Table 2) and remained unaffected by the presence of oxygen. The prompt component generally is between 0 and 35 ns [41]. The shortest lifetime was observed for compound DB17. This can be explained by the smaller transition energy which facilitated higher nonradiative paths. This is also proven by the lowest PLQY from

all investigated compounds. Similarly, as for emission spectra, the alkyl chain did not significantly influence the excited state lifetime. The delay component ranged from 150 to 180 μs, reflecting the relatively large difference between the singlet and triplet energy levels, which limits RISC. The estimation of the delayed component had a large error of about 30 μs due to the short observation time. Nonetheless, the presence of a delayed component supports the TADF mechanism.

3.4. Energy Levels

Ionization and electron affinity energy are presented in Table 3. The length of alkyl chains did not influence the ionization energy of the compound. Small changes are related to the measurement error. Electron affinity energy was more affected by the length of the alkyl chain, but no systematic changes in dependence on alkyl chain length were observed. This could mean that these changes are more affected by the arrangement of the molecule in the film. In the case of a symmetric molecule (DB17), both energy levels were lower than in an unsymmetrical molecule (DB26). Benzophenone was minimally affected by the ionization energy because it is mainly determined by the electron-donating groups. At the same time, the level of electron affinity was much lower, which indicates a greater ability to trap electrons.

Table 3. Ionization and electron affinity energy of investigated compounds in thin films.

Compounds	Ionization Energy, eV (±0.03 eV)	Electron Affinity Energy, eV (±0.06 eV)
DB16	5.28	2.43
DB17	5.30	2.70
DB18	5.43	2.68
DB22	5.45	2.50
DB26	5.40	2.55
DB27	5.40	2.60

The studied compounds have a relatively high level of electron affinity; therefore, when creating an OLED structure, it is necessary to choose an electron transport material that will be able to provide a good electron transfer. Therefore, 2,2′,2″-(1,3,5-benzinetriyl)-tris(1-phenyl-1-H-benzimidazole) (TPBi), whose electron affinity energy is 2.7 eV, was taken as the electron transport material in the OLED structure (see Figure S17).

3.5. Characterization of OLED

Organic light-emitting diodes with the following structure were prepared using the studied compounds: ITO/PEDOT:PSS (40 nm)/emitter (50 nm)/TPBi (25 nm)/LiF (1 nm)/Al (120 nm). The performance of the best devices is shown in Table S2. The best results were exhibited by compounds DB16 and DB17, which, with symmetric carbazole groups despite its lower PLQY, demonstrates notable brightness, whereas DB16 closely approaches a pure blue color, as evident from its x, y coordinates in the CIE 1931 color space of (0.17, 0.16) and Figure 6. On the other hand, DB17 has coordinates of (0.26; 0.39), indicating a greenish-yellow emission (see Figure 6).

The turn-on voltage for both compounds is relatively low. Specifically, DB16 and DB17 exhibit turn-on voltages of 3.2 V and 2.6 V in devices, respectively, which align with the results reported in the literature [42]. The lower turn-on voltage of DB17 can be attributed to its emission occurring closer to the green light spectrum. Although the turn-on voltage and CIE color coordinates show competitive results, the efficiency is relatively low.

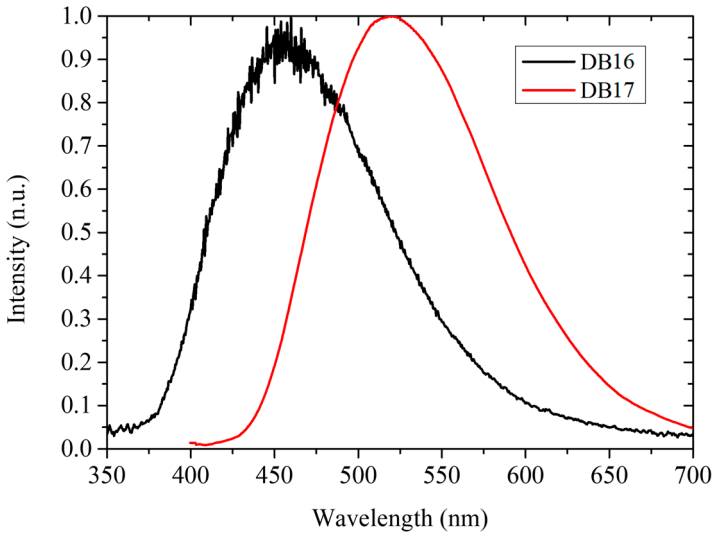

Figure 6. Electroluminescence spectra of compounds DB16 and DB17.

4. Conclusions

Six novel organic emitters, incorporating carbazole electron-donating groups and diphenyl sulfone or benzophenone electron acceptors, were synthesized and characterized. It was established that these derivatives exhibit high thermal stability and amorphous characteristics, forming stable thin films with glass transition temperatures ranging from 77 °C to 147 °C. Quantum chemical calculations revealed minimal overlap between the HOMO and LUMO, suggesting potential TADF properties. These materials emit light in the deep blue or blue-green regions, with photoluminescence quantum yields exceeding 50% in degassed solutions. Notably, the intensity of emission diminishes in non-degassed solvents. The difference between the singlet and triplet energy was in the range from 0.14 to 0.22 eV, indicating the possibility of reverse intersystem crossing. The photoluminescence kinetics consist of two decay components: prompt and delayed. The delayed component diminishes in non-degassed solution, providing further evidence of a potential TADF effect. Two of the compounds exhibited promising performance in organic light-emitting devices. Material DB16, based on diphenyl sulfone and emitting in the deep blue region, exhibited a turn-on voltage of 4.0 V and a maximum brightness of 178 cd/m^2 when applied as an emitter in devices. Meanwhile, DB17, a derivative based on benzophenone and emitting in the blue-green region, demonstrated a turn-on voltage of 3.5 V and a maximum luminance of 660 cd/m^2 when utilized as an emitter in OLEDs. A further optimization of the emitter structures and a reduction in HOMO-LUMO overlap could enhance the performance of these diodes. Additionally, OLED devices were fabricated under standard laboratory conditions, and efficiency could be improved by optimizing device structures and layer thicknesses. This research underscores the potential of diphenyl sulfone, benzophenone, and bicarbazole fragments as promising building blocks for efficient TADF emitters in future applications.

Supplementary Materials: The following supporting information can be downloaded at https://www.mdpi.com/article/10.3390/coatings14101294/s1, Figures S1–S6: 1H NMR spectra of material; Figures S7–S12: TGA curve of compounds; Table S1. Absorption and emission peaks in THF solution and pure thin films; Figure S13: Molecular orbital positions of HOMO and LUMO levels for investigated molecules; Figure S14: Emission spectra of all compounds in degassed (black line) and non-degassed (red line) THF solution; Figure S15: Fluorescence spectra of thin films taken at room temperature (red solid line) and phosphorescence spectra of thin films taken at 77 K with 100 μs delay (black dashed line); Figure S16: Photoluminescence kinetics of compounds in degassed (black line) and non-degassed (red line) THF solution; Figure S17: Energy level diagram of prepared OLEDs. Table S2: Electroluminescence characteristics of the fabricated best devices, a at max brightness. Ref. [43] is cited in the supplementary materials.

Author Contributions: Conceptualization, A.V. and S.G.; methodology, M.A.Z., R.G. and D.B.; software, A.P.; formal analysis, M.A.Z., A.V. and D.T.; investigation, M.A.Z., N.T., R.G., D.B. and G.K.; writing—original draft preparation, M.A.Z.; writing—review and editing, A.V., D.T. and S.G.; visualization, M.A.Z.; supervision, A.V. and S.G.; funding acquisition, A.V. and S.G. All authors have read and agreed to the published version of the manuscript.

Funding: This work was supported by the Research Council of Lithuania (Grant No. S-LLT-19-2). This work was supported by VIAA project No. 1.1.1.2/VIAA/4/20/592. This work was supported by the M era Net 2019 call project "Enabling a Commercially Viable Long Lifespan and High Efficiency Omni Friendly OLED Lighting Source with G2 and G3 Emitters". Institute of Solid-State Physics, University of Latvia, received funding from the European Union's Horizon 2020 Framework Programme H2020-WIDESPREAD-01-2016-2017-TeamingPhase2 under grant agreement No. 739508, project CAMART^2.

Institutional Review Board Statement: Not applicable.

Informed Consent Statement: Not applicable.

Data Availability Statement: The data presented in this study are available on request from the corresponding author.

Conflicts of Interest: The authors declare no conflict of interest.

References

1. Sun, K.; Sun, Y.; Jiang, W.; Huang, S.; Tian, W.; Sun, Y. Highly Efficient and Color Tunable Thermally Activated Delayed Fluorescent Emitters and Their Applications for the Solution-Processed OLEDs. *Dye. Pigment.* **2017**, *139*, 326–333. [CrossRef]
2. Chen, H.-W.; Lee, J.-H.; Lin, B.-Y.; Chen, S.; Wu, S.-T. Liquid Crystal Display and Organic Light-Emitting Diode Display: Present Status and Future Perspectives. *Light. Sci. Appl.* **2017**, *7*, 17168. [CrossRef] [PubMed]
3. Hsiang, E.; Yang, Z.; Yang, Q.; Lan, Y.; Wu, S. Prospects and Challenges of Mini-LED, OLED, and Micro-LED Displays. *J. Soc. Inf. Disp.* **2021**, *29*, 446–465. [CrossRef]
4. Vasilopoulou, M.; Mohd Yusoff, A.R.B.; Daboczi, M.; Conforto, J.; Gavim, A.E.X.; da Silva, W.J.; Macedo, A.G.; Soultati, A.; Pistolis, G.; Schneider, F.K.; et al. High Efficiency Blue Organic Light-Emitting Diodes with below-Bandgap Electroluminescence. *Nat. Commun.* **2021**, *12*, 4868. [CrossRef] [PubMed]
5. Ying, S.; Liu, W.; Peng, L.; Dai, Y.; Yang, D.; Qiao, X.; Chen, J.; Wang, L.; Ma, D. A Promising Multifunctional Deep-Blue Fluorophor for High-Performance Monochromatic and Hybrid White OLEDs with Superior Efficiency/Color Stability and Low Efficiency Roll-Off. *Adv. Opt. Mater.* **2022**, *10*, 2101920. [CrossRef]
6. Tankelevičiūtė, E.; Samuel, I.D.W.; Zysman-Colman, E. The Blue Problem: OLED Stability and Degradation Mechanisms. *J. Phys. Chem. Lett.* **2024**, *15*, 1034–1047. [CrossRef]
7. Siddiqui, I.; Kumar, S.; Tsai, Y.-F.; Gautam, P.; Shahnawaz; Kesavan, K.; Lin, J.-T.; Khai, L.; Chou, K.-H.; Choudhury, A.; et al. Status and Challenges of Blue OLEDs: A Review. *Nanomaterials* **2023**, *13*, 2521. [CrossRef]
8. Lee, C.W.; Lee, J.Y. Above 30% External Quantum Efficiency in Blue Phosphorescent Organic Light-Emitting Diodes Using Pyrido[2,3- *b*]Indole Derivatives as Host Materials. *Adv. Mater.* **2013**, *25*, 5450–5454. [CrossRef]
9. Adachi, C.; Baldo, M.A.; Thompson, M.E.; Forrest, S.R. Nearly 100% Internal Phosphorescence Efficiency in an Organic Light-Emitting Device. *J. Appl. Phys.* **2001**, *90*, 5048–5051. [CrossRef]
10. Yang, X.; Yue, L.; Yu, Y.; Liu, B.; Dang, J.; Sun, Y.; Zhou, G.; Wu, Z.; Wong, W. Strategically Formulating Aggregation-Induced Emission-Active Phosphorescent Emitters by Restricting the Coordination Skeletal Deformation of Pt(II) Complexes Containing Two Independent Monodentate Ligands. *Adv. Opt. Mater.* **2020**, *8*, 2000079. [CrossRef]
11. Liu, D.; Ren, H.; Deng, L.; Zhang, T. Synthesis and Electrophosphorescence of Iridium Complexes Containing Benzothiazole-Based Ligands. *ACS Appl. Mater. Interfaces* **2013**, *5*, 4937–4944. [CrossRef] [PubMed]
12. Mei, Y.; Lan, Y.; Li, D.; Wang, J.; Xie, L.; Peng, X.; Li, J.; Liu, D.; Su, S.-J. Hydrogen Bond Boosts EQEs to 30+% for Acridone-Carbazole Based Deep-Blue TADF Emitters in Simple-Structure OLEDs. *Chem. Eng. J.* **2024**, *480*, 148351. [CrossRef]
13. Kim, E.; Park, J.; Jun, M.; Shin, H.; Baek, J.; Kim, T.; Kim, S.; Lee, J.; Ahn, H.; Sun, J.; et al. Highly Efficient and Stable Deep-Blue Organic Light-Emitting Diode Using Phosphor-Sensitized Thermally Activated Delayed Fluorescence. *Sci. Adv.* **2022**, *8*, eabq1641. [CrossRef] [PubMed]
14. Luo, X.-F.; Xiao, X.; Zheng, Y.-X. Recent Progress in Multi-Resonance Thermally Activated Delayed Fluorescence Emitters with an Efficient Reverse Intersystem Crossing Process. *Chem. Commun.* **2024**, *60*, 1089–1099. [CrossRef] [PubMed]
15. Kumar, K. High-Efficiency Functional Materials: Challenges and Developments in Solution and Dry Processed Green OLEDs. *React. Chem. Eng.* **2024**, *9*, 496–527. [CrossRef]

16. Oner, S.; Bryce, M.R. A Review of Fused-Ring Carbazole Derivatives as Emitter and/or Host Materials in Organic Light Emitting Diode (OLED) Applications. *Mater. Chem. Front.* **2023**, *7*, 4304–4338. [CrossRef]
17. Naveen, K.R.; Lee, H.; Braveenth, R.; Karthik, D.; Yang, K.J.; Hwang, S.J.; Kwon, J.H. Achieving High Efficiency and Pure Blue Color in Hyperfluorescence Organic Light Emitting Diodes Using Organo-Boron Based Emitters. *Adv. Funct. Mater.* **2022**, *32*, 2110356. [CrossRef]
18. Kaji, H.; Suzuki, H.; Fukushima, T.; Shizu, K.; Suzuki, K.; Kubo, S.; Komino, T.; Oiwa, H.; Suzuki, F.; Wakamiya, A.; et al. Purely Organic Electroluminescent Material Realizing 100% Conversion from Electricity to Light. *Nat. Commun.* **2015**, *6*, 8476. [CrossRef]
19. Goushi, K.; Yoshida, K.; Sato, K.; Adachi, C. Organic Light-Emitting Diodes Employing Efficient Reverse Intersystem Crossing for Triplet-to-Singlet State Conversion. *Nat. Photonics* **2012**, *6*, 253–258. [CrossRef]
20. Wang, L.; Li, T.; Feng, P.; Song, Y. Theoretical Tuning of the Singlet–Triplet Energy Gap to Achieve Efficient Long-Wavelength Thermally Activated Delayed Fluorescence Emitters: The Impact of Substituents. *Phys. Chem. Chem. Phys.* **2017**, *19*, 21639–21647. [CrossRef]
21. Woo, J.Y.; Park, M.; Jeong, S.; Kim, Y.; Kim, B.; Lee, T.; Han, T. Advances in Solution-Processed OLEDs and Their Prospects for Use in Displays. *Adv. Mater.* **2023**, *35*, 2207454. [CrossRef] [PubMed]
22. Zhang, M.; Zheng, C.-J.; Lin, H.; Tao, S.-L. Thermally Activated Delayed Fluorescence Exciplex Emitters for High-Performance Organic Light-Emitting Diodes. *Mater. Horiz.* **2021**, *8*, 401–425. [CrossRef] [PubMed]
23. Nagar, M.R.; Kumar, K.; Blazevicius, D.; Beresneviciute, R.; Krucaite, G.; Tavgeniene, D.; Hao, C.T.; Banik, S.; Jou, J.-H.; Grigalevicius, S. Solution Processable Carbazole-Benzophenone Derivatives as Bipolar Hosts Enabling High-Efficiency Stable Green TADF Organic LEDs. *J. Mater. Chem. C Mater.* **2023**, *11*, 1579–1592. [CrossRef]
24. Zheng, Q.; Wang, X.-Q.; Qu, Y.-K.; Xie, G.; Liao, L.-S.; Jiang, Z.-Q. Solution-Processable through-Space Charge-Transfer Emitters via Solubilizing Groups Modification. *Npj Flex. Electron.* **2022**, *6*, 83. [CrossRef]
25. Lee, G.H.; Kim, Y.S. High-Efficiency Diphenylsulfon Derivative-Based Organic Light-Emitting Diode Exhibiting Thermally-Activated Delayed Fluorescence. *J. Korean Phys. Soc.* **2016**, *69*, 398–401. [CrossRef]
26. Xia, Y.; Li, J.; Chen, X.; Li, A.; Guo, K.; Chen, F.; Zhao, B.; Chen, Z.; Wang, H. Molecular Engineering of Push-Pull Diphenylsulfone Derivatives towards Aggregation-Induced Narrowband Deep Blue Thermally Activated Delayed Fluorescence (TADF) Emitters. *Chem.–A Eur. J.* **2022**, *28*, e202202434. [CrossRef]
27. Bas, E.E.; Ulukan, P.; Monari, A.; Aviyente, V.; Catak, S. Photophysical Properties of Benzophenone-Based TADF Emitters in Relation to Their Molecular Structure. *J. Phys. Chem. A* **2022**, *126*, 473–484. [CrossRef]
28. Bezvikonnyi, O.; Gudeika, D.; Volyniuk, D.; Mimaite, V.; Sebastine, B.R.; Grazulevicius, J.V. Effect of Donor Substituents on Thermally Activated Delayed Fluorescence of Diphenylsulfone Derivatives. *J. Lumin.* **2019**, *206*, 250–259. [CrossRef]
29. Pocock, I.A.; Alotaibi, A.M.; Jagdev, K.; Prior, C.; Burgess, G.R.; Male, L.; Grainger, R.S. Direct Formation of 4,5-Disubstituted Carbazoles *via* Regioselective Dilithiation. *Chem. Commun.* **2021**, *57*, 7252–7255. [CrossRef]
30. Wex, B.; Kaafarani, B.R. Perspective on Carbazole-Based Organic Compounds as Emitters and Hosts in TADF Applications. *J. Mater. Chem. C Mater.* **2017**, *5*, 8622–8653. [CrossRef]
31. Ledwon, P. Recent Advances of Donor-Acceptor Type Carbazole-Based Molecules for Light Emitting Applications. *Org. Electron.* **2019**, *75*, 105422. [CrossRef]
32. Whitten, J.E. Ultraviolet Photoelectron Spectroscopy: Practical Aspects and Best Practices. *Appl. Surf. Sci. Adv.* **2023**, *13*, 100384. [CrossRef]
33. Kane, E.O. Theory of Photoelectric Emission from Semiconductors. *Phys. Rev.* **1962**, *127*, 131–141. [CrossRef]
34. Gao, Y. Surface Analytical Studies of Interfaces in Organic Semiconductor Devices. *Mater. Sci. Eng. R Rep.* **2010**, *68*, 39–87. [CrossRef]
35. Kanai, K.; Honda, M.; Ishii, H.; Ouchi, Y.; Seki, K. Interface Electronic Structure between Organic Semiconductor Film and Electrode Metal Probed by Photoelectron Yield Spectroscopy. *Org. Electron.* **2012**, *13*, 309–319. [CrossRef]
36. Frisch, M.J.; Trucks, G.W.; Schlegel, H.B.; Scuseria, G.E.; Robb, M.A.; Cheeseman, J.R.; Scalmani, G.; Barone, V.; Mennucci, B.; Petersson, G.A.; et al. *Gaussian 09, Revision D.01*; Gaussian. Inc.: Wallingford, CT, USA, 2009.
37. Turek, A.M.; Krishnamoorthy, G.; Phipps, K.; Saltiel, J. Resolution of Benzophenone Delayed Fluorescence and Phosphorescence with Compensation for Thermal Broadening. *J. Phys. Chem. A* **2002**, *106*, 6044–6052. [CrossRef]
38. Serevičius, T.; Skaisgiris, R.; Kreiza, G.; Dodonova, J.; Kazlauskas, K.; Orentas, E.; Tumkevičius, S.; Juršėnas, S. TADF Parameters in the Solid State: An Easy Way to Draw Wrong Conclusions. *J. Phys. Chem. A* **2021**, *125*, 1637–1641. [CrossRef]
39. Li, C.; Harrison, A.K.; Liu, Y.; Zhao, Z.; Zeng, C.; Dias, F.B.; Ren, Z.; Yan, S.; Bryce, M.R. Asymmetrical-Dendronized TADF Emitters for Efficient Non-doped Solution-Processed OLEDs by Eliminating Degenerate Excited States and Creating Solely Thermal Equilibrium Routes. *Angew. Chem. Int. Ed.* **2022**, *61*, e202115140. [CrossRef]
40. Yi, R.; Liu, G.; Luo, Y.; Wang, W.; Tsai, H.; Lin, C.; Shen, H.; Chang, C.; Lu, C. Dicyano-Imidazole: A Facile Generation of Pure Blue TADF Materials for OLEDs. *Chem. A Eur. J.* **2021**, *27*, 12998–13008. [CrossRef]
41. Shi, H.; Jing, W.; Liu, W.; Li, Y.; Li, Z.; Qiao, B.; Zhao, S.; Xu, Z.; Song, D. Key Factors Governing the External Quantum Efficiency of Thermally Activated Delayed Fluorescence Organic Light-Emitting Devices: Evidence from Machine Learning. *ACS Omega* **2022**, *7*, 7893–7900. [CrossRef]

42. Li, B.; Li, Z.; Hu, T.; Zhang, Y.; Wang, Y.; Yi, Y.; Guo, F.; Zhao, L. Highly Efficient Blue Organic Light-Emitting Diodes from Pyrimidine-Based Thermally Activated Delayed Fluorescence Emitters. *J. Mater. Chem. C Mater.* **2018**, *6*, 2351–2359. [CrossRef]
43. Romero, D.B.; Schaer, M.; Zuppiroli, L.; Leclerc, M.; Ades, D.; Siove, A. The role of carbazole in organic light-emitting devices. *Synth. Met.* **1996**, *80*, 271–277. [CrossRef]

Disclaimer/Publisher's Note: The statements, opinions and data contained in all publications are solely those of the individual author(s) and contributor(s) and not of MDPI and/or the editor(s). MDPI and/or the editor(s) disclaim responsibility for any injury to people or property resulting from any ideas, methods, instructions or products referred to in the content.